



Trans. Nonferrous Met. Soc. China 35(2025) 3455-3467

Transactions of Nonferrous Metals Society of China

www.tnmsc.cn



# Effect of joint coalescence coefficient on rock bridge formation of slope based on finite difference method

Su LI, Yi TANG, Hang LIN

School of Resources and Safety Engineering, Central South University, Changsha 410083, China

Received 24 January 2024; accepted 20 September 2024

**Abstract:** A method combining finite difference method (FDM) and k-means clustering algorithm which can determine the threshold of rock bridge generation is proposed. Jointed slope models with different joint coalescence coefficients (k) are constructed based on FDM. The rock bridge area was divided through k-means algorithm and the optimal number of clusters was determined by sum of squared errors (SSE) and elbow method. The influence of maximum principal stress and stress change rate as clustering indexes on the clustering results of rock bridges was compared by using Euclidean distance. The results show that using stress change rate as clustering index is more effective. When the joint coalescence coefficient is less than 0.6, there is no significant stress concentration in the middle area of adjacent joints, that is, no generation of rock bridge. In addition, the range of rock bridge is affected by the coalescence coefficient (k), the relative position of joints and the parameters of weak interlayer.

**Key words:** slope; rock bridge; finite difference method; k-means algorithm

### 1 Introduction

Due to external influences such as natural wind erosion, earthquake, rainfall and artificial excavation, a large number of joints, faults and weak interlayers are formed inside the slopes, with different sizes and complex spatial distribution [1–4]. These joints and weak interlayers seriously damage the structural integrity of the slope, and greatly reduce the stability of slope [5–7]. Once the slope is subjected to strong external interference (seismic shock, blasting vibration caused by artificial excavation, etc), cracks will develop rapidly from the original stable joint tips inside the slope [8-11]. Two or more joints and weak interlayers in close proximity will connect with each other and form a macroscopic failure plane, resulting in the destabilization of slope, and triggering a variety of geological disasters [12–14]. For example, in Qianjiangping, China, a large number of joints exist inside the slope. Under the influence of heavy rainfall, the physical properties of the slope, such as cohesion, decreased obviously [15]. The joints within the slope developed rapidly and connected with each other to form a sliding surface.

In a slope, rock bridge is regarded as the rock section between adjacent joints, which hinders the expansion of joint (Fig. 1) [16,17]. It avoids the coalescence of multiple joints to form a macroscopic sliding surface, which is an important geological structure to maintain the stability of slope [18]. Influenced by self-weight and shearing, the rock bridge will be in a highly concentrated state of stress, and a large amount of deformation energy has been accumulated inside it [19,20]. Therefore, once the rock bridge is damaged, the slope will collapse instantly and form a high-speed debris flow landslide, causing serious environmental

damage and casualties [21]. In Chongqing, southwestern China, a large amount of kinetic energy was released after the destruction of rock bridges in the Cocktail Mountains [22]. The landslide was characterized by a high velocity debris flow, which posed a significant threat to the safety of surrounding people and the ecosystem.

For this reason, many scholars have carried out research on the effect of rock bridge on rock stability and achieved a series of remarkable results. SARFARAZI and HAERI [23] quantitatively investigated the effect of the number, area and configuration of rock bridges on their shear properties based on experiments. Some scholars adopted different methods to investigate the effect of rock bridge geometrical parameters on its mechanical parameters and failure characteristics [24,25]. HUANG et al [26] studied the influence of rock bridge on slope failure modes by Particle Flow

Code (PFC) and proposed a formula for calculating the slope safety factor considering rock bridge. TUCKEY and STEAD [27] used remote sensing and field surveys to evaluate the morphology of rock bridges in slopes.

Rock bridge is the key factor to control slope stability. ELMO et al [28] argues that rock bridge cannot be defined simply as the rock section between two discontinuous joint. In Fig. 2(a), according to the traditional definition of a rock bridge, a rock bridge of length  $L_1$  occurs between two short joints. In fact, if the length of two joints is very short and the distance between them is exceptionally far, the two joints will not coalescence with each other. The rock section between them will not be in a state of high stress concentration, which means that rock bridge is not created. In this case, the damage of the slope itself,

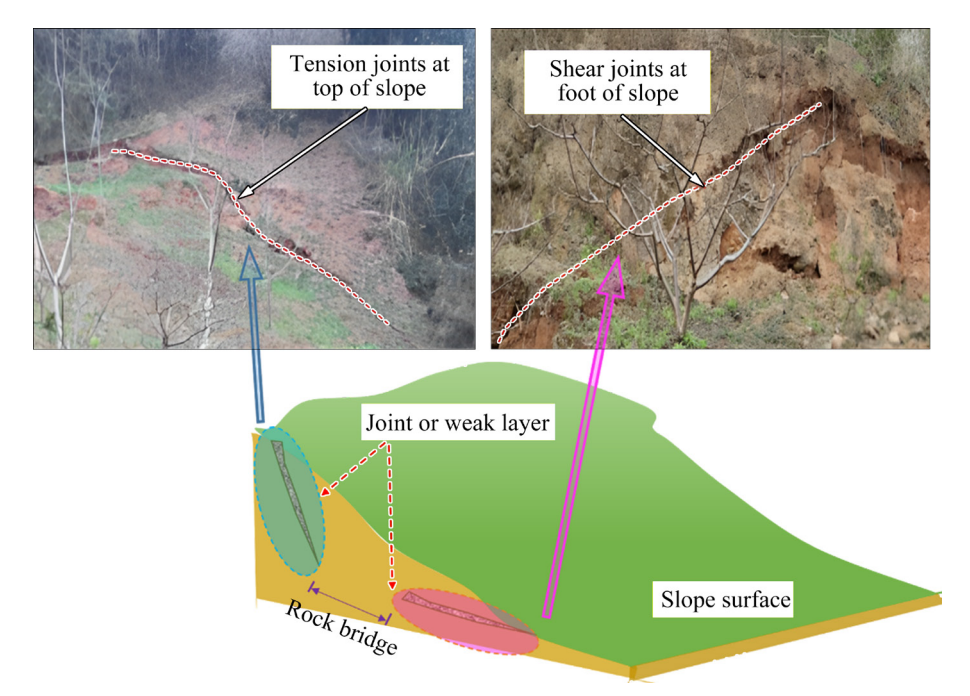


Fig. 1 Joints and rock bridges in slopes

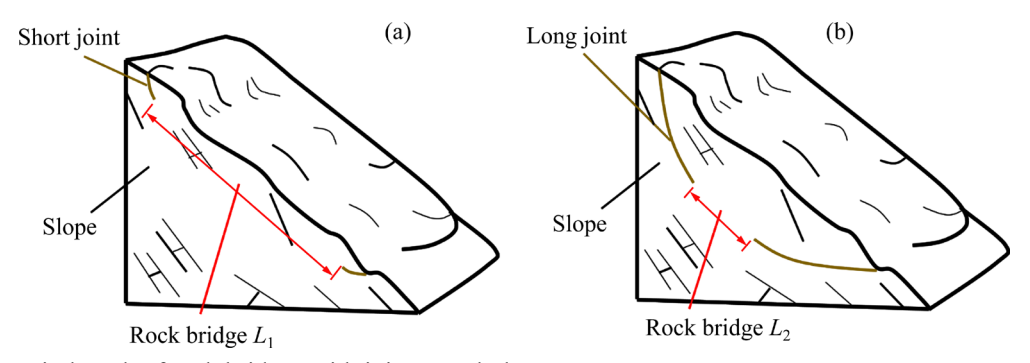


Fig. 2 Changes in length of rock bridges with joint morphology

such as gravity, internal friction angle, and cohesion. On the contrary, if the length of two joints is very long and the ligament length is short (Fig. 2(b)), the rock bridge between them will form a high stress concentration state to hinder the connection of the joints. Once the bridge is disturbed and damaged, the slope will collapse instantly to form a landslide disaster. At this time, the damage depends more on the physical properties of the rock bridge (length, angle, etc). Previously, the way of defining rock bridge depended only on the position of the joint tips. Therefore, how to effectively distinguish the formation and shape of rock bridge between joints is of great significance for slope warming.

In this work, a method to determine the threshold value for rock bridge generation is proposed. Combined with the damage morphology of engineering slopes, slope models with different coalescence coefficients (k) are constructed by finite difference method (FDM). Based on the characteristics of high stress in the rock bridge area, the k-means clustering algorithm is introduced, and the maximum principal stress of each grid in the slope and the stress change rate are taken as the indexes of clustering, and the clustering effect of these two indexes is compared. The clustering results of rock bridge based on FDM and k-means algorithm were verified by the theory of maximum circumferential tensile stress. Finally, multiple sets of slope models with different joint coalescence coefficients (k) were constructed and the threshold value for rock bridge generation was determined. The threshold value of rock bridge generation is affected by the joint length, the relative position of joints and the parameters of weak interlayer. The method proposed in this work can quickly and effectively determine whether there is a rock bridge generated within the slope (i.e., a high stress area) and determine the range of the rock bridge. The high stress characteristics of rock bridge can make people understand the slope state more clearly and quickly, so as to improve the efficiency of slope warning.

### 2 Method for identifying rock bridge length

In the existing studies, researchers usually take the rock section between adjacent joints as rock bridge, and the length of the connecting line between adjacent joint tips as ligament length. In fact, a number of parameters, such as the ratio of ligament length to joint length and the joint angle, are related to the formation of rock bridge. If the joint geometric parameters can be used to determine whether rock bridges (areas of stress concentration) have been generated, it can help engineers better assess the risk of slope failure and establish construction scheme safely. A method incorporating rock bridges into slope stability assessment was proposed [29]. Since the slope destabilization needs to consider the effects of rock bridge and discontinuous joints, the slope is destabilized only after the rock bridges have been damaged by shearing (Fig. 2). According to Ref. [29], ligament length can be expressed as a joint coalescence coefficient (k) (Fig. 3). This coefficient describes the ratio of the length of rock bridge,  $L_R$ , to the length of idealized sliding surface,  $L_{\rm S}$ , and joint length,  $L_{\rm J}$ .

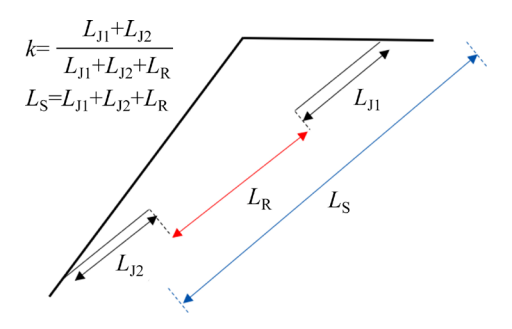


Fig. 3 Schematic calculation of joint coalescence coefficient (k)

### 2.1 Establishment of jointed slope models

A numerical model of the slope as shown in Fig. 4 was established with reference to Figs. 1 and 2. Two weak interlayers are arranged at the top and foot of the slope, respectively, and the line length connecting the endpoints of the two weak interlayers was regarded as ligament length. The length of the potential damage surface is 20 m, the length of the rock bridge is 4 m and 16 m, the total length of the joint is 16 m and 4 m, and the continuity coefficients (k) are 0.2 and 0.8, respectively. In addition, due to the elongated shape of the weak interlayer, the mesh density around the weak interlayer is increased in order to improve the computational accuracy. Other parameters of the model are shown in Fig. 4. In Table 1 and Fig. 4, E is the elastic modulus, c is the cohesion, v is the

Poisson's ratio,  $\varphi$  is the internal friction angle,  $\gamma$  is the gravity, and g is the acceleration of gravity. The bottom length of the slope is 40 m, the height is 20 m and the slope angle is 45°.

#### 2.2 Maximum principal stress in slope

The cohesion (c) and internal friction angle  $(\varphi)$  of rock mass are divided by a reduction factor  $(F_s)$  to obtain the virtual parameters  $(c_f \text{ and } \varphi_f)$  (Eq. (1)). Under the action of  $c_f$  and  $\varphi_f$ , the value of  $F_s$  is varied until the slope is in critical equilibrium state, and the value of  $F_s$  at this time represents the safety factor of the slope:

$$c_{\rm f} = \frac{c}{F_{\rm s}}, \ \varphi_{\rm f} = \tan^{-1}(\tan\varphi/F_{\rm s}) \tag{1}$$

Figure 5 illustrates the maximum principal stress distribution of two slopes with coalescence coefficients equal to 0.2 and 0.8 under the limit equilibrium stat. The overall stress distribution of two slopes is approximately the same. For slope with k=0.8, there is an obvious stress concentration in rock section between two weak interlayers. For slope with k=0.2, there is no stress concentration in rock section between two weak interlayers. It can be proven that when the distance between two weak

**Table 1** Physical parameters of different parts in slope model

Location	E/MPa	c/kPa	v	$arphi/(^\circ)$	$\gamma/(kN\cdot m^{-3})$	$g/(\text{m}\cdot\text{s}^{-2})$
Slope	$10^{3}$	250	0.25	23	27	9.8
Weak interlayer	10	1	0.33	7	17	

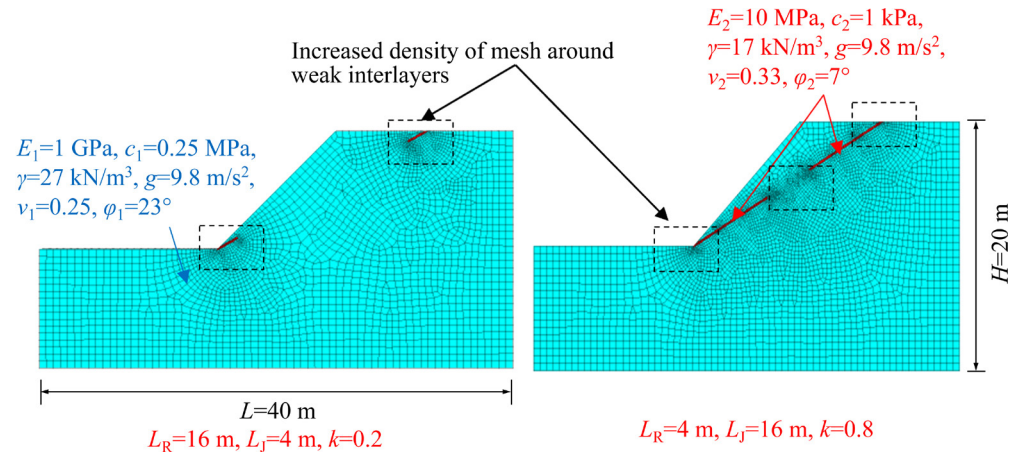


Fig. 4 Two slope models with different joint coalescence coefficients

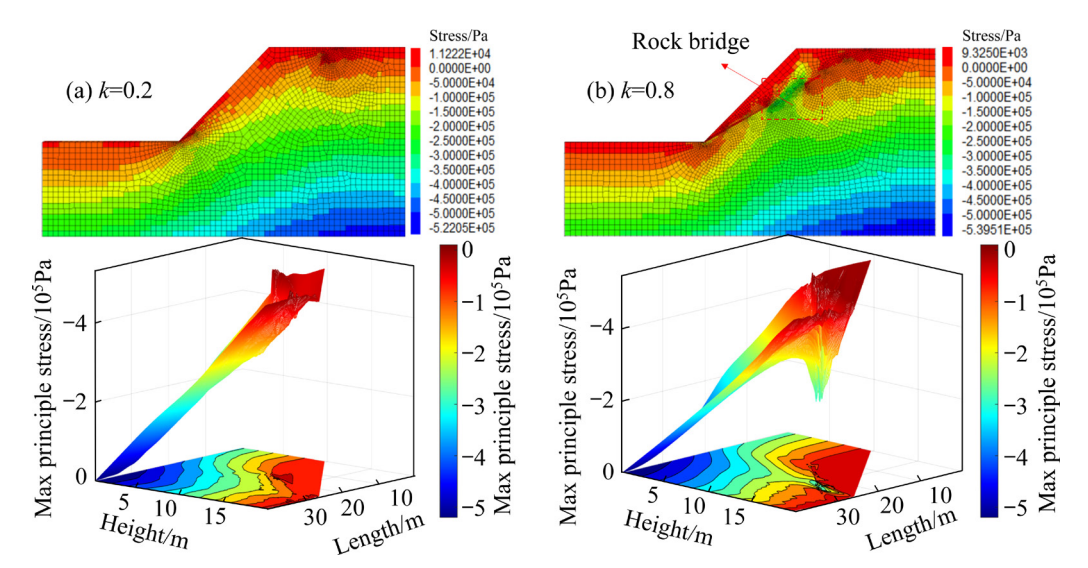


Fig. 5 Distribution of maximum principal stress in slopes with different joint coalescence coefficients: (a) k=0.2; (b) k=0.8

interlayers exceeds a threshold value, the rock between them does not produce stress concentration. In Fig. 5(b), the maximum principal stress of rock bridge is much higher than that of its surrounding rock mass, so it is possible to see by eye that there is an obvious stress concentration, and then judge whether the rock bridge is formed or not. However, when the stress of rock bridge is close to the surrounding rock, this subjective judgment by naked eyes will have a large deviation. Therefore, the *k*-means algorithm is introduced to identify automatically whether the rock bridge has been formed.

### 2.3 Rock bridge area recognition based on k-means algorithm

The *k*-means algorithm is a widely used clustering algorithm that categorizes data into multiple clusters based on the magnitude of difference between different data [30,31].

- (1) It is known that there are m grids in the slope model, the coordinates of each grid  $G_i$  are  $(x_i, y_i)$ , and the corresponding maximum principal stress is  $\sigma_i$ . Set the number of clusters as cluster\_k and the location of the cluster center as  $C_i$ .
- (2) The Euclidean distance was employed to compute the distance between the stress  $\sigma_i$  of grid  $G_i$  (i=1, 2,  $\cdots$ , m) and the stress  $\sigma_j$  of respective cluster centers  $C_j$  (j=1, 2,  $\cdots$ , cluster\_k). If the mesh  $G_i$  (i=m-1) has the shortest distance from the cluster center  $C_j$  (j=cluster\_k-1), then  $G_i$  is added to the cluster of  $C_j$ . The Euclidean distance is calculated as

$$Dist_{Ed}(G_i, C_j) = |\sigma(G_i) - \sigma(C_i)|$$
 (2)

(3) After assigning all grids to each clustering center, the first clustering is completed. Calculate the average of the maximum principal stress of the n grids  $G_i$  contained in the clustering center  $C_j$  and use this average as the new clustering center  $C_{j_new}$ :

$$C_{j_{\text{new}}} = \frac{\sum_{i=1}^{n} \sigma(G_i)}{n}$$
(3)

(4) Repeat Steps (2) and (3) until the difference between  $C_{j_{\text{new}}}$  and  $C_j$  is less than a given threshold, which is  $1 \times 10^{-5}$ . This indicates that the grid within the newly generated  $C_{j_{\text{new}}}$  is almost the same as the mesh within  $C_j$ . The clustering result converges and the clustering cycle ends.

$$\sqrt{\sum_{j=1}^{k} (C_{j_{-\text{new}}} - C_{j})^{2}} < 1 \times 10^{-5}$$
 (4)

(5) In addition, the elbow method and the sum of squared errors (SSE) are combined to determine the optimal number of cluster k:

$$SSE = \sum_{j=1}^{k} \sum_{G_{j,i} \in C_j} |G_{j,i} - C_j|^2$$
 (5)

 $G_{j,i}$  denotes the *i*th grid in cluster  $C_j$ . The SSE decreases as the number of clusters increases. But too many clusters will make the clustering results distorted. By using elbow method (Fig. 6), the point where SSE decreases from fast to slow is selected as the best number of clusters.

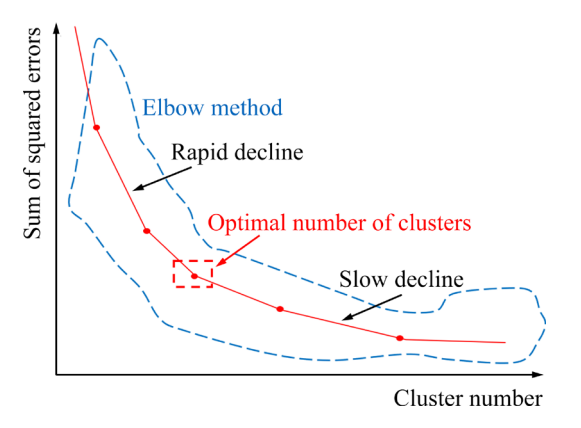


Fig. 6 Sketch of using elbow method to choose optimal cluster number

The coordinate  $(x_i, y_i)$  and maximum principal stress  $\sigma_i$  of all grids in the slope are brought into the k-means algorithm. Equation (2) is used to calculate the distance between the grids, Eq. (3) is applied to updating the center of clusters, Eq. (4) is employed to determine whether the results are convergent or not, and the number of cluster\_k is set to be from 2 to 10 (Fig. 7).

Figure 7 illustrates the result of the slope clustering with different cluster\_k, with each color representing a category (The clustering result for cluster\_k=1 is not meaningful and therefore is not shown in Fig. 7). It can be clearly seen that there is an ellipse-like structure between two weak interlayers of the slope when cluster\_k=4. The location of this structure is consistent with a rock bridge, and the stress distribution is obviously higher than that of the surrounding rock. Therefore, it can be assumed that the elliptical structure is the rock bridge. When cluster\_k is less than 4, the rock

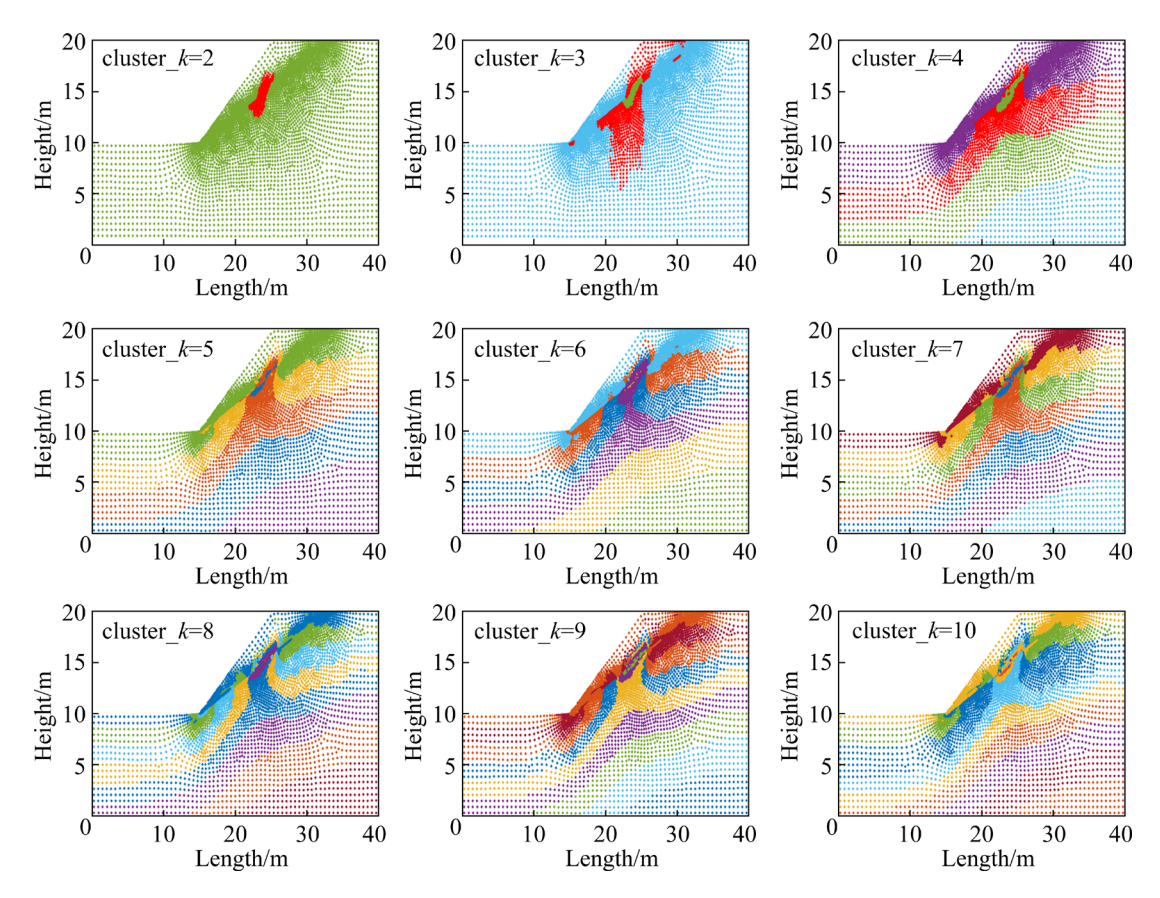


Fig. 7 Effect of different cluster number on clustering results of rock bridge area in slope

bridge is not successfully clustered, and when k is greater than 4, there are too many clusters, which leads to distorted results. From Fig. 7, the optimal cluster\_k for this clustering should be 4. To validate this result, Eq. (5) was used to calculate the SSE and the elbow method was used to further determine the optimal cluster\_k (Fig. 8). Figure 8 illustrates the SSE due to different values of cluster\_k. When cluster\_k=1, all the meshes inside the slope are classified as a cluster, and the difference between the maximum principal stress of each mesh is so large that the SSE reaches a maximum value of  $4.28 \times 10^8$ . Combined with the elbow method, the optimal cluster\_k for this clustering is 4.

The maximum principal stress can be used to characterize the stress concentration phenomenon of rock bridge. However, it can be clearly seen in Fig. 7 that there are some meshes inside the rock bridge that are divided into other clusters during the clustering process, and there are rock masses at the bottom of the slope that are divided into the same cluster as the rock bridge. Although the stress inside the rock bridge is greater than that of surrounding

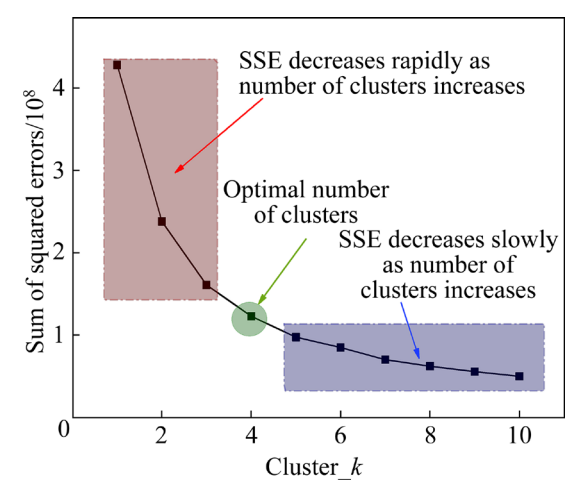


Fig. 8 Relationship between sum of squared errors (SSE) and cluster k

rock, the rock mass at the bottom of the slope will also be in a state of high stress under the action of gravity, so there will be quite a lot of rock mass and rock bridge in the same stress range. Therefore, these rock masses at the bottom of the slope will be in the same cluster as the rock bridge, while a small amount of meshes inside the rock bridge will be divided into other clusters (Fig. 9).

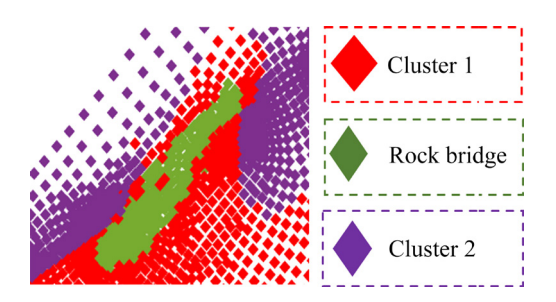


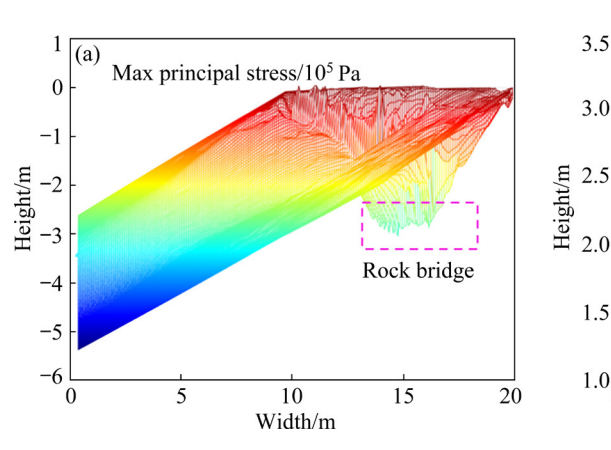
Fig. 9 Some meshes inside rock bridge classified into other clusters by using maximum principal stress as indicator for clustering

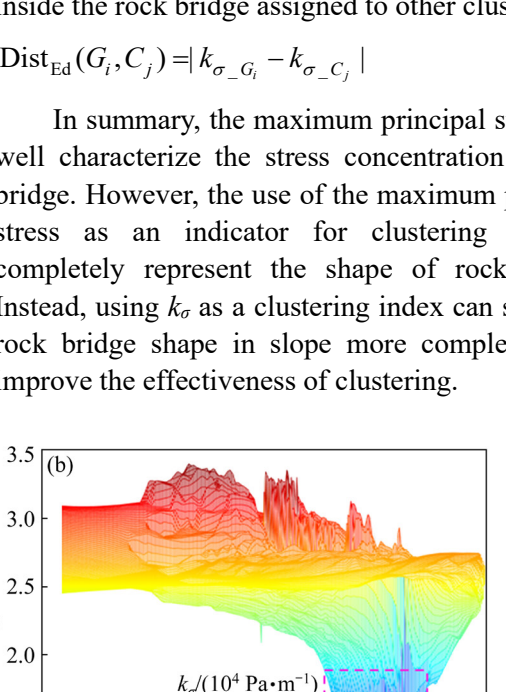
#### 2.4 Variation of maximum principal stress

From Fig. 5, it can be seen that the maximum principal stress at the bottom of the slope will higher than the stress within the rock bridge due to the influence of slope height. Since the maximum principal stress value cannot highlight the stress concentration characteristics of rock bridge well, the stress change rate  $k_{\sigma}$  is introduced as another clustering index. Assuming that there is a grid G<sub>i</sub> in the slope, the grid  $G_{i1}$  at the bottom of slope is found to be the closest to the grid  $G_i$  in the x-direction (Fig. 10). The expression for the value of  $k_{\sigma i}$  for the grid  $G_i$  is given in Eq. (6):

$$k_{\sigma i} = \frac{|\sigma_i - \sigma_{i1}|}{\sqrt{(x_i - x_{i1})^2 + (y_i - y_{i1})^2}}$$
(6)

The  $k_{\sigma}$  values corresponding to all grids in the slope were calculated, and a 3D cloud map of the coordinates versus the  $k_{\sigma}$  was plotted (Fig. 11). As can be seen from Fig. 11(b), the  $k_{\sigma}$  of the rock bridge is much lower than that of other rock masses in the slope.  $k_{\sigma}$  can better characterize the variability of rock bridge itself than the maximum principal stress.





Rock bridge

10

Width/m

15

20

5

Fig. 11 Comparison of 3D cloud maps of maximum principal stress (a) and rate of stress change  $(k_{\sigma})$  (b) versus slope height

3.0

1.5

1.00

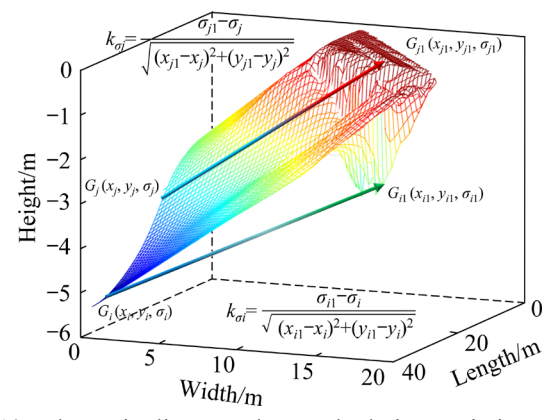


Fig. 10 Schematic diagram about calculating variation of max principal stress  $k_{\sigma}$ 

Therefore, the  $k_{\sigma}$  was brought into the k-means algorithm as new index for clustering, and the Euclidean distance was used as the formula (Eq. (7)). The clustering results are shown in Fig. 12. By comparing Fig. 12(a) and Fig. 12(b), it is obvious that the shape of rock bridges obtained by clustering using  $k_{\sigma}$  as an indicator is much more regular and there is no mesh inside the rock bridge assigned to other clusters. While the clustered rock bridge using maximum principal stress as an indicator has a stranger shape and there are meshes inside the rock bridge assigned to other clusters:

$$\operatorname{Dist}_{\operatorname{Ed}}(G_{i}, C_{i}) = |k_{\sigma_{i}} - k_{\sigma_{i}}| \tag{7}$$

In summary, the maximum principal stress can well characterize the stress concentration of rock bridge. However, the use of the maximum principal stress as an indicator for clustering fails to completely represent the shape of rock bridge. Instead, using  $k_{\sigma}$  as a clustering index can show the rock bridge shape in slope more completely and improve the effectiveness of clustering.

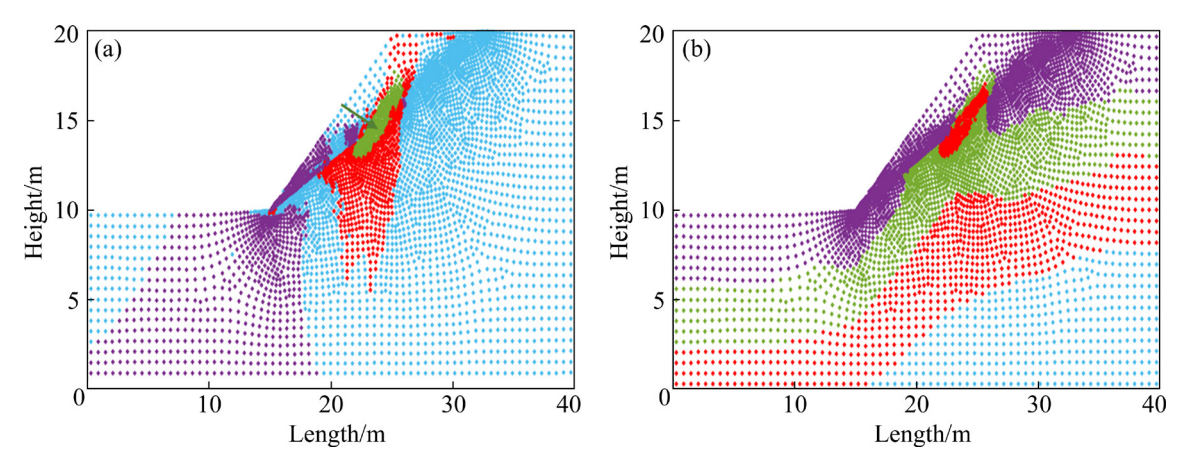
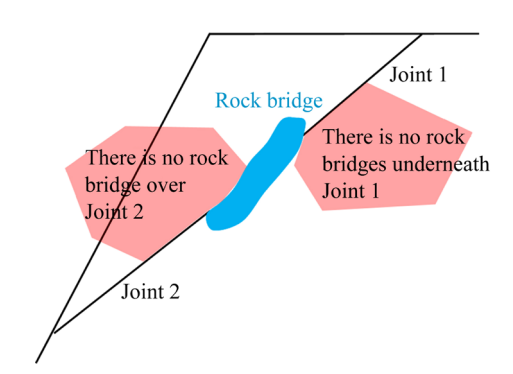


Fig. 12 Comparison of clustering results of rock bridge by using different indicators: (a) Using  $k_{\sigma}$  as indicator; (b) Using maximum principal stress as indicator

## 3 Proof of clustering results for rock bridge

From Fig. 12, it can be found that the rock bridge is located between two joints, but the distribution between the two joints is irregular. It can be clearly seen that the right end of the rock bridge is above Joint 1 and the left end of the rock bridge is below Joint 2 (Fig. 13). The irregular distribution of rock bridge can be explained by maximum circumferential tensile stress theory.



**Fig. 13** Relationship between location of joints and rock bridge

According to maximum circumferential tensile stress theory [21], an assumed circumferential stress field exists at the crack tip and the circumferential tensile stress ( $\sigma_{\theta}$ ) is not the same everywhere in that circumferential stress field. The crack will extend and expand in the direction of the maximum  $\sigma_{\theta}$ :

$$\frac{\partial \sigma_{\theta}}{\partial \theta} = 0, \ \frac{\partial^2 \sigma_{\theta}}{\partial \theta^2} < 0 \tag{8}$$

The polar expression for the stress near the crack tip is given in Eq. (9) and Fig. 14:

$$\begin{cases}
\sigma_{r} = \frac{1}{2\sqrt{2\pi r}} \left[K_{I}(3 - \cos\theta)\cos\frac{\theta}{2} + K_{II}(3\cos\theta - 1)\sin\frac{\theta}{2}\right] \\
K_{II}(3\cos\theta - 1)\sin\frac{\theta}{2}\right] \\
\sigma_{\theta} = \frac{1}{2\sqrt{2\pi r}}\cos\frac{\theta}{2} \left[K_{I}\cos^{2}\frac{\theta}{2} - \frac{3}{2}K_{II}\sin\theta\right] \\
\tau_{r\theta} = \frac{1}{2\sqrt{2\pi r}}\cos\frac{\theta}{2} \left[K_{I}\sin\theta + K_{II}(3\cos\theta - 1)\right]
\end{cases}$$
(9)

Substituting Eq. (9) into Eq. (8) gives

$$\frac{\partial \sigma_{\theta}}{\partial \theta} = \frac{-3}{4\sqrt{2\pi r}} \cos \frac{\theta}{2} [K_{\rm I} \sin \theta + K_{\rm II} (3\cos \theta - 1)]$$
 (10)

" $\cos(\theta/2)=0$ " is the solution to Eq. (10). However, when  $\theta=\pm\pi$ , the crack will expand along the direction of original joint, and this solution has no practical significance. Thus, Eq. (10) is simplified to Eq. (11):

$$K_{\rm I}\sin\theta + K_{\rm II}(3\cos\theta - 1) = 0 \tag{11}$$

 $K_{\rm I}$  and  $K_{\rm II}$  are the stress intensity factors for Type I and Type II cracks, respectively.  $\theta$  is the angle between the newly created crack and the original joint. If the crack is a pure Type I crack,  $K_{\rm II}$ =0 and  $\theta$ =0°. If the crack is a pure Type II crack,  $K_{\rm I}$ =0 and  $\theta$ =70.52° (Eq. (11)). Therefore, for normal mixed Type I and II cracks, the angle between the newly created crack and the original joint is between 0° and 70.52° (Fig. 15).

According to Fig. 15, it can be seen that cracks will be generated in the lower right part of the Joint

1, so this part of the area will not be a concentration area of stress. Similarly, the upper left side of Joint 2 will not be a concentration of stress. Therefore, the rock bridge will not be distributed in these two areas.

### 4 Length threshold for rock bridge formation

The rock bridge is clustered in Sections 2 and 3, and the clustering result is verified using the maximum circumferential stress theory. The length threshold for rock bridge formation will be further

determined in Section 4. Based on the slope model in Fig. 3, the coalescence coefficient (k) is set to be 0.2, 0.3, 0.4, 0.5, 0.6, 0.7, 0.8, and 0.9, respectively. The slope models with different k values are shown in Fig. 16.

Figure 17 illustrates the clustering results for slopes with different coalescence coefficients (k). It can be seen that there exists rock bridge between joints when k is in the range of 0.7–0.9, while there is no generation of rock bridge when k is in the range of 0.2–0.6. It can be concluded that when the ratio of two joints length to ligament length is less than a certain value, the rock bridge will not be

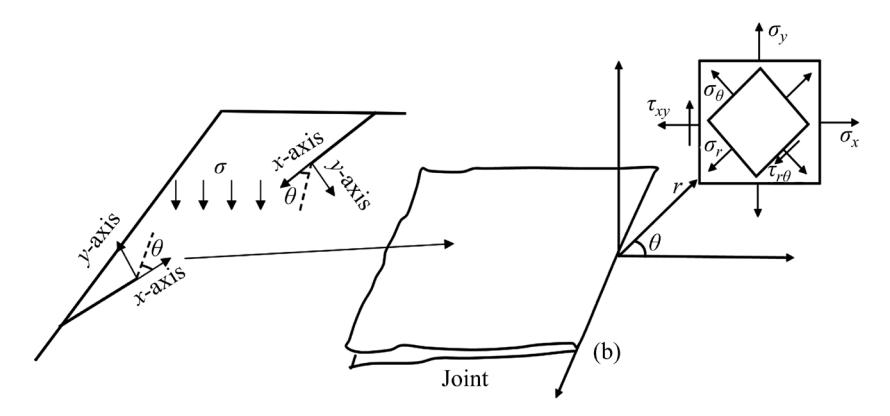


Fig. 14 Polarized stress components near crack tip

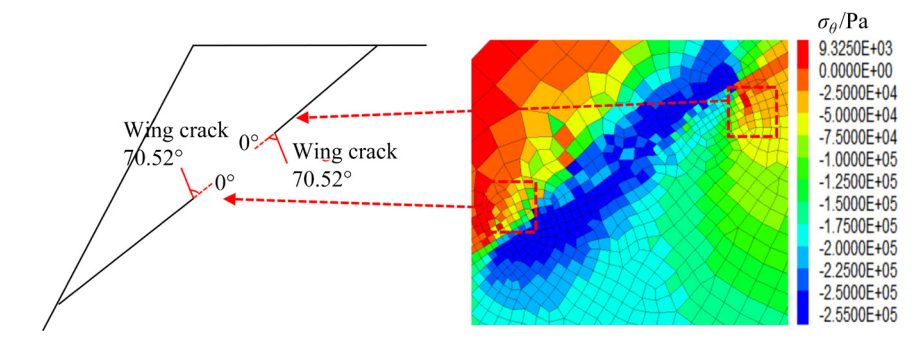


Fig. 15 Comparison of simulation result with theoretical result based on maximum circumferential tensile stress theory

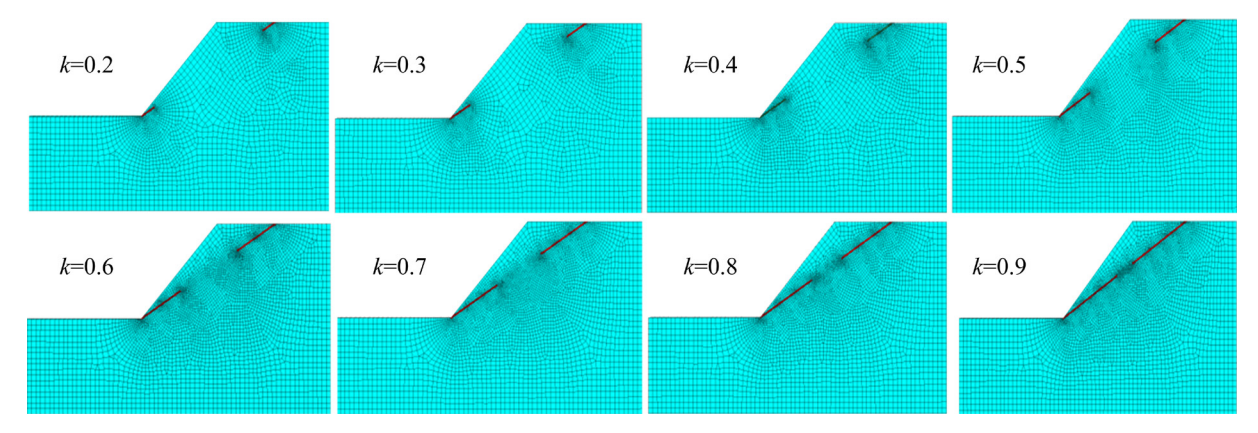


Fig. 16 Slope models with different coalescence coefficients (k)

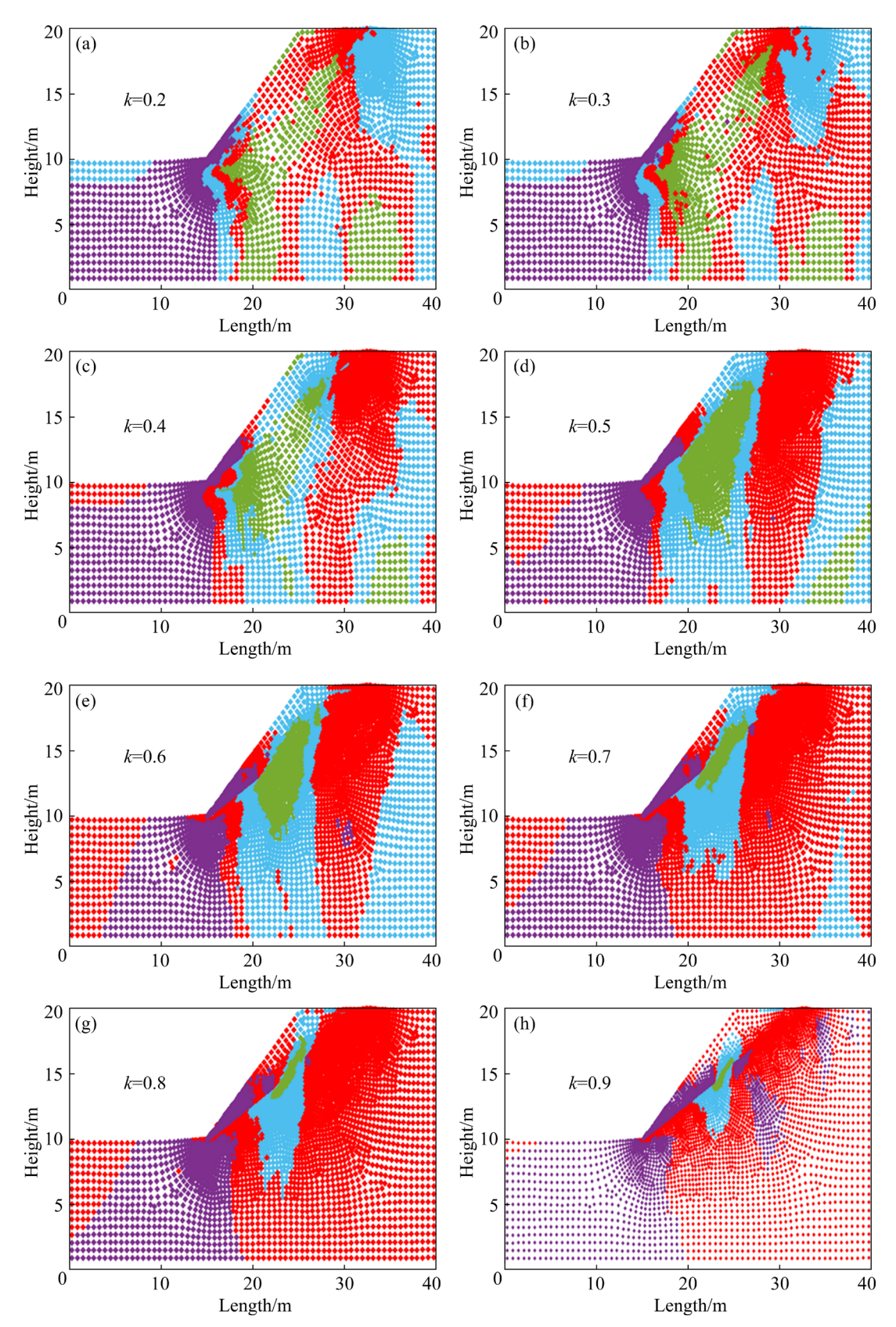


Fig. 17 Effect of different coalescence coefficient (k) on clustering results of rock bridge

generated. Figure 17 shows that the regular stress concentration inside the rock bridge occurs only when k is in the range of 0.6–0.7. Therefore, in the

model established in this work, the threshold of k which leads to the generation of rock bridge is about 0.6-0.7.

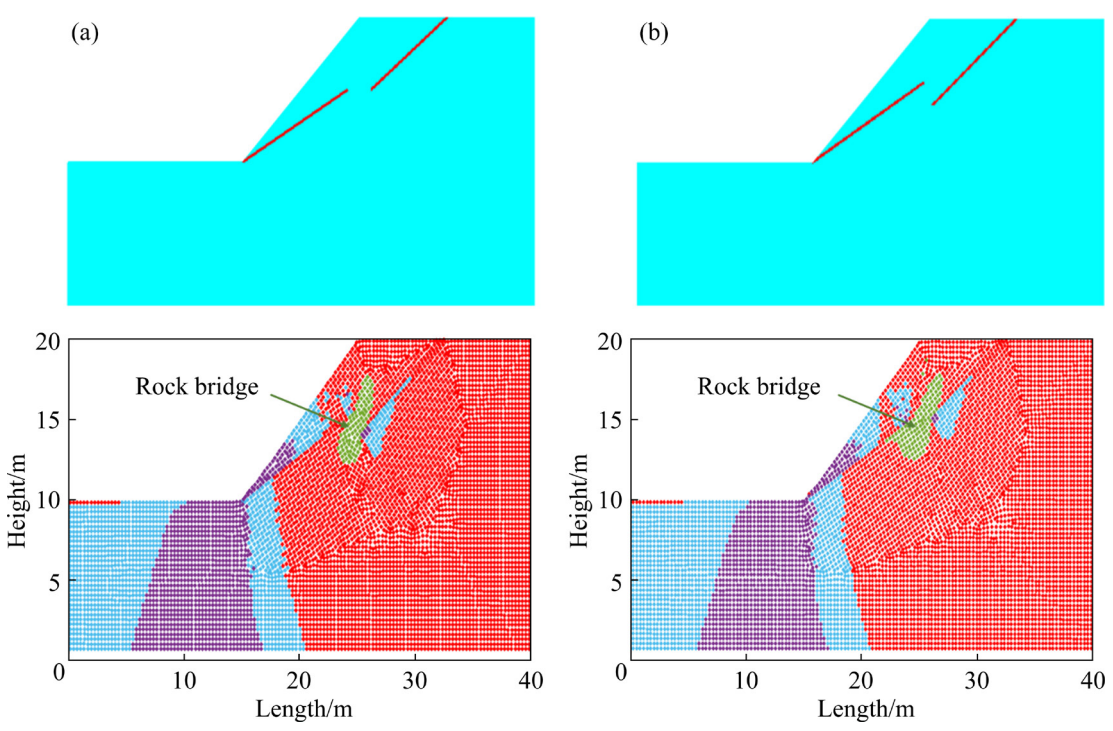


Fig. 18 Range of rock bridge in non-collinear weak interlayers: (a) Ligament angle of 0°; (b) Ligament angle of 90°

This work focuses on the generation of rock bridge between collinear weak interlayers. For non-collinear weak interlayers, rock bridge can still be generated between them. Compared with the slope with collinear weak interlayers, the threshold k leading to the generation of rock bridge in the slope with non-collinear weak interlayers is also different (Fig. 18). In Fig. 18, the clustering results of rock bridge between two non-collinear weak interlayers show that the relative position of weak interlayer also affects the range of rock bridge. In addition, the clustering results of rock bridge are also affected by the parameters of the weak interlayer. For example, the higher the cohesion of the weak interlayer, the lower the load to be carried by the rock bridge, and the stress concentration phenomenon is not obvious. In summary, it can be seen that the threshold value for the generation of rock bridges is affected by the length of the joints, the relative position of the joints, and the mechanical parameters of weak interlayer (Fig. 18). In addition, the stresses of each mesh in the numerical model of the slope are derived to calculate the length of the rock bridge. Therefore, the calculation results in this work are highly dependent on the accuracy of the simulation results of FDM. If the simulation results of FDM are inaccurate and differ significantly from the actual

results, the credibility of the conclusions obtained in this work will also decrease.

### **5 Conclusions**

- (1) By combining the FDM and *k*-means clustering algorithms, a method for determining the threshold for rock bridge generation is proposed. The method can be applied to engineered slopes with different joints.
- (2) Influenced by the gravity and size of the slope itself, the variation of stress highlights the stress concentration in rock bridge more than the maximum principal stress. The threshold for rock bridge generation and the range of rock bridge varies with the coalescence coefficient (k), the relative position of joints, and the mechanical parameters of weakly interlayer.
- (3) Rock bridge cannot be thought of simply as rock sections between neighboring joints. When two joints are far apart, there is no high stress concentration and no coalescence between two joints, which means that no rock bridge is generated.

#### **CRediT** authorship contribution statement

**Su LI:** Writing – Original draft preparation, Writing – Reviewing & editing, Conception, Visualization; **Yi** 

**Tang:** Writing – Original draft preparation, Writing – Reviewing & editing, Visualization, Investigation; **Hang LIN:** Funding acquisition, Validation, Data curation.

### **Declaration of competing interest**

The authors declare that they have no known competing financial interests or personal relationships that could have appeared to influence the work reported in this paper.

### **Data Availability**

The data used to support the findings of this study are available from the corresponding author upon request.

### Acknowledgments

This work was supported by the National Natural Science Foundation of China (No. 42277175); Guangxi Emergency Management Department 2024 Innovation Technology Research Project, China 2024GXYJ006); Hunan Provincial Department of Natural Resources Geological Exploration Project, China (No. 2023ZRBSHZ056); The First National Natural Disaster Comprehensive Risk Survey in Hunan Province, China (No. 2022-70); Guizhou Provincial Major Technological Scientific and Program, China (No. 2023-425).

### References

- [1] CHANG Wen-bin, WANG Ping, XING Ai-guo, WANG Hui-juan, YU Yi-fan, LI Xu-dong. Failure mode and dynamic response of loess slopes with tectonic joints under seismic action [J]. Environmental Earth Sciences, 2021, 80: 531.
- [2] YANG Heng-tao, BAI Bing, LIN Hang. Seismic magnitude calculation based on rate- and state-dependent friction law [J]. Journal of Central South University, 2023, 30: 2671–2685.
- [3] LIANG Zu-chao, WANG Dong, LI Guang-he, SUN Guang-yu, YU Ming-yu, XIA Dong, DING Chun-jian. Three-dimensional stability calculation method for high and large composite slopes formed by mining stope and inner dump in adjacent open pits [J]. International Journal of Mining Science and Technology, 2024, 34: 507–520.
- [4] LI Guang-he, YANG Xiao-xu, WANG Dong, WANG Yan-ting, YU Xiang-yu. Stability of inner dump slope under coal pillar support: case study in an open-pit coal mine [J]. International Journal of Coal Science & Technology, 2022, 9: 25.
- [5] LI Su, LIN Hang, LIN Qi-bin, WANG Yi-xian, ZHAO Yan-lin, HU Hui-hua. Mechanical behavior and failure characteristics of double-layer composite rock-like specimens with two coplanar joints under uniaxial loading

- [J]. Transactions of Nonferrous Metals Society of China, 2023, 33: 2815-2831.
- [6] SUN Lei, GRASSELLI G, LIU Quan-sheng, TANG Xu-hai, ABDELAZIZ A. The role of discontinuities in rock slope stability: Insights from a combined finite-discrete element simulation [J]. Computers and Geotechnics, 2022, 147: 104788.
- [7] ZARE S, KARIMI-NASAB S, JALALIFAR H. Analysis and determination of the behavioral mechanism of rock bridges using experimental and numerical modeling of non-persistent rock joints [J]. International Journal of Rock Mechanics and Mining Sciences, 2021, 141: 104714.
- [8] LIAN Ji-jian, LI Qin, DENG Xi-fei, ZHAO Gao-feng, CHEN Zu-yu. A numerical study on toppling failure of a jointed rock slope by using the distinct lattice spring model [J]. Rock Mechanics and Rock Engineering, 2018, 51: 513-530.
- [9] CHEN Yi-fan, SHENG Bi-yang, XIE Shi-jie, CAO Ri-hong, WANG Yi-xian, ZHAO Yan-lin, LIN Hang. Crack propagation and scale effect of random fractured rock under compression—shear loading [J]. Journal of Materials Research and Technology, 2023, 23: 5164–5180.
- [10] LIU Bo, CHEN Yi-fan, LIN Hang, CAO Ri-hong, ZHANG Sheng-wen. Experimental study on shear behavior of rock composite material under normal unloading conditions [J]. Materials, 2023, 16: 1233.
- [11] GAO Ru-gao, WANG Wei-jun, XIONG Xin, LI Jing-jing, XU Chun. Effect of curing temperature on the mechanical properties and pore structure of cemented backfill materials with waste rock-tailings [J]. Construction and Building Materials, 2023, 409: 133850.
- [12] KOSTIC S. Analytical models for estimation of slope stability in homogeneous intact and jointed rock masses with a single joint [J]. International Journal of Geomechanics, 2017, 17: 04017089.
- [13] ZHAO Lian-heng, YU Cheng-hao, CHENG Xiao, ZUO Shi, JIAO Kang-fu. A method for seismic stability analysis of jointed rock slopes using Barton-Bandis failure criterion [J]. International Journal of Rock Mechanics and Mining Sciences, 2020, 136: 104487.
- [14] LIU Zhi-zhen, CAO Ping, LIN Hang, MENG Jing-jing, WANG Yi-xian. Three-dimensional upper bound limit analysis of underground cavities using nonlinear Baker failure criterion [J]. Transactions of Nonferrous Metals Society of China, 2020, 30: 1916–1927.
- [15] WANG Jin-ge, SCHWEIZER D, LIU Qing-bing, SU Ai-jun, HU Xin-li, BLUM P. Three-dimensional landslide evolution model at the Yangtze River [J]. Engineering Geology, 2021, 292: 106275.
- [16] CHEN Yi-fan, LIN Hang, CAO Ri-hong, ZHANG Chun-yang. Slope stability analysis considering different contributions of shear strength parameters [J]. International Journal of Geomechanics, 2021, 21: 04020265.
- [17] CHEN Hong-ran, QIN Si-qing, XUE Lei, YANG Bai-cun, ZHANG Ke. A physical model predicting instability of rock slopes with locked segments along a potential slip surface [J]. Engineering Geology, 2018, 242: 34–43.
- [18] YUE Zhu-feng, MENG Fan-zhen, ZHOU Xiong, WANG Xiao-shan, ZHANG Li-ming, WANG Zai-quan. Influence of

- non-persistent joint aperture and inclination angle on the shear behavior and fracture mode of solid rock and concrete material [J]. Construction and Building Materials, 2022, 316: 125892.
- [19] TANG Peng, CHEN Guo-qing, HUANG Run-qiu, WANG Dong. Effect of the number of coplanar rock bridges on the shear strength and stability of slopes with the same discontinuity persistence [J]. Bulletin of Engineering Geology and the Environment, 2021, 80: 3675–3691.
- [20] DELONCA A, GUNZBURGER Y, VERDEL T. Cascade effect of rock bridge failure in planar rock slides: Numerical test with a distinct element code [J]. Natural Hazards and Earth System Sciences, 2021, 21: 1263–1278.
- [21] CHEN Guo-qing, LIU Hui, QIN Chang-an, ZHAO Cong, HUANG Run-qiu. Mechanical properties and crack model of central rock bridge in triaxial unloading test [J]. Chinese Journal of Rock Mechanics and Engineering 2017, 36: 1162–1173.
- [22] TANG Yi, LIN Hang, CAO Ri-hong, SUN Shu-wei, ZHA Wen-hua. Role of rock sections in intermittent joints in controlling rock mass strength and failure modes [J]. Rock Mechanics and Rock Engineering, 2023, 56: 5203–5221.
- [23] SARFARAZI V, HAERI H. Effect of number and configuration of bridges on shear properties of sliding surface [J]. Journal of Mining Science, 2016, 52: 245–257.
- [24] BU Feng-chang, XUE Lei, ZHAI Meng-yang, XU Chao, CUI Yuan. Numerical investigation of the scale effects of rock bridges [J]. Rock Mechanics and Rock Engineering,

- 2022, 55: 5671–5685.
- [25] TANG Peng, CHEN Guo-qing, HUANG Run-qiu, ZHU Jing. Brittle failure of rockslides linked to the rock bridge length effect [J]. Landslides, 2020, 17: 793–803.
- [26] HUANG Da, CEN Duo-feng, MA Guo-wei, HUANG Run-qiu. Step-path failure of rock slopes with intermittent joints [J]. Landslides, 2015, 12: 911–926.
- [27] TUCKEY Z, STEAD D. Improvements to field and remote sensing methods for mapping discontinuity persistence and intact rock bridges in rock slopes [J]. Engineering Geology, 2016, 208: 136–153.
- [28] ELMO D, STEAD D, YANG B, MARCATO G, BORGATTI L. A new approach to characterise the impact of rock bridges in stability analysis [J]. Rock Mechanics and Rock Engineering, 2022, 55: 2551–2569.
- [29] ZHENG Bo-wen, QI Sheng-wen, Guo Song-feng, HUANG Xiao-lin, LIANG Ning, ZOU Yu, LUO Guang-ming. A new shear strength criterion for rock masses with non-persistent discontinuities considering the nonlinear progressive failure process [J]. Materials, 2020, 13: 4694.
- [30] L ABIODUN M, E ABSALOM E, A LAITH, A BELAL, JIA He-ming. K-means clustering algorithms: A comprehensive review, variants analysis, and advances in the era of big data [J]. Information Sciences, 2023, 622: 178–210.
- [31] SINAGA K P, YANG Miin-shen. Unsupervised k-means clustering algorithm [J]. IEEE Access, 2020, 8: 80716-80727.

### 基于有限差分法的节理连通率对边坡岩桥形成的影响

李骕,汤艺,林杭

中南大学 资源与安全工程学院,长沙 410083

摘 要:结合有限差分法(FDM)和 k 均值聚类算法,提出了一种用于确定岩桥生成阈值的方法。基于 FDM 构建了具备不同节理贯通率(k)的节理边坡模型。采用 k 均值算法对岩桥区域进行划分,并采用误差平方和(SSE)和时部法则确定最优簇数。通过欧拉距离比较了以最大主应力值和应力变化率为聚类指标对岩桥聚类结果的影响。结果表明,以应力变化率作为聚类指标更为准确有效。当节理贯通率小于 0.6 时,相邻节理的中间区域不存在明显应力集中,即无岩桥形成。此外,岩桥范围受节理贯通率、节理相对位置和弱夹层参数的影响。

关键词: 边坡; 岩桥; 有限差分法; k均值算法

(Edited by Bing YANG)